Reversible pH-Controlled Catenation of a Benzobisimidazole-based Tetranuclear Rectangle

Maksym Dekhtiarenko, Simon Pascal, Mourad Elhabiri, Valérie Mazan, David Canevet, Magali Allain, Vincent Carré, Frédéric Aubriet, Zoia Voitenko, Marc Sallé, et al.

Reversible pH-Controlled Catenation of a Benzobisimidazole-based Tetranuclear Rectangle

Maksym Dekhtiarenko,[a],[e] Simon Pascal,*[b] Mourad Elhabiri,[c] Valerie Mazan,[c] David Canevet,[a] Magali Allain,[a] Vincent Carré,[d] Frédéric Aubriet,[d] Zoia Voitenko,[e] Marc Sallé,*[a] Olivier Siri,*[b] and Sébastien Goeb*[a]

Abstract: The development of methodologies to control on demand and reversibly supramolecular transformations from self-assembled metalla-structures requires the rational design of architectures able to answer to an applied stimulus. While solvent, concentration, guest, light, addition of a chemical have been largely explored to provide these transformations, the case of pH sensitive materials is less described. Herein, we report the first example of a pH-triggered dissociation of a coordination-driven self-assembled interlocked molecular link. It incorporates a pH sensitive benzobisimidazole-based ligand that can be selectively protonated on its bisimidazole moieties. This generates intermolecular electrostatic repulsions that reduces drastically the stability of the interlocked structure, leading to its dissociation without any sign of protonation of the basic pyridine moieties involved in the coordination bonds. Importantly, the dissociation process is reversible through addition of a base.

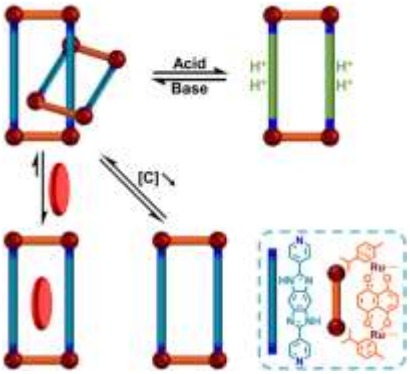

The coordination-driven self-assembly strategy, supported both by the highly predictable directionality of the metal-ligand interaction and by the reversible nature of the coordination bond, is remarkably efficient when targeting the construction of sophisticated discrete rings and cages.[1] Those systems inherently feature a cavity prone to interfere in host-guest chemistry[2] with potential applications in catalysis,[3] sensing[4] or drug delivery.[5] In principle, they also enable to reach intricate interlocked systems. While several synthetic methodologies towards metalla-macrocycles and cages have been described, the reasoned preparation of interlocked architectures, *i.e.* molecular links[6] (*e.g.* catenanes,[7] ring-in-ring complexes,[8] Solomon links,[9] Trefoil Knots[9b, 10] or Borromean rings[11] to cite a few) or interpenetrated cage structures,[12] remains a challenge since decreasing the number of independent species is entropically unfavorable. Several parameters can help in achieving the locking process by providing an extra enthalpic energy such as for example π–π stacking, electrostatic or hydrogen-bonding interactions, as well as solvophobic effects.[13] On the other hand, controlling reversibly the supramolecular transformation of coordination-driven architectures focuses much attention.[14] This could be achieved upon *i)* changing solvent or concentration,[11b] *ii)* adding a chemical, *i.e.* a competitive component[9b] or a guest template,[6b] or *iii)* using a light[15] or redox[16] physicochemical stimulation. Scarce examples of pH-sensitive architectures have been depicted to monitor the supramolecular transformation between metalla-structures. They mostly explore the Brønsted-base character of the binding pyridine units and the resulting competing metal coordination / protonation processes, allowing to drive for host's disassembly[17] in a context of guest release[16a, 18] or switching between non interlocked metalla-structures.[19] To the best of our knowledge, no pH-driven supramolecular transformation has been depicted yet through assistance of alternative pH-sensitive groups.

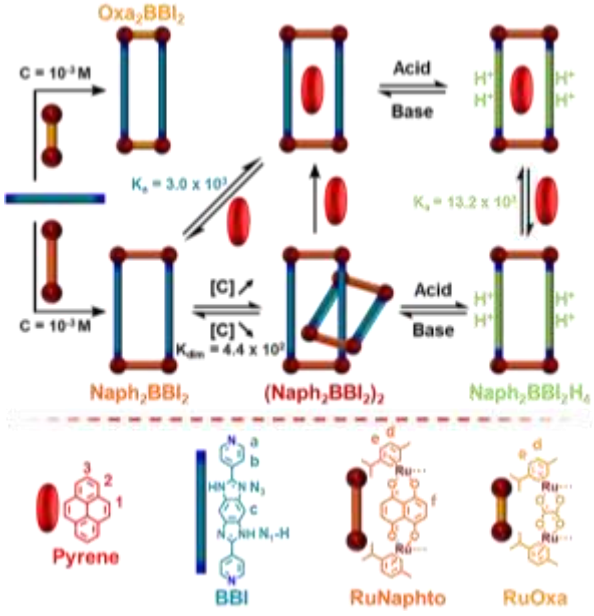

Figure 1. Synthesis of the self-assembled metalla-rectangles **Oxa$_2$BBI$_2$** and **Naph$_2$BBI$_2$** from the benzobisimidazole ligand (**BBI**) and the bis-ruthenium complexes (**RuOxa** or **RuNaphto**), and subsequent supramolecular transformations occurring in MeOD from **Naph$_2$BBI$_2$**.

[a] M. Dekhtiarenko, Dr. D. Canevet, M. Allain, Prof. M. Sallé, Dr. S. Goeb
Univ Angers, CNRS, MOLTECH-Anjou, 2 bd Lavoisier, F-49045 Angers, France.
E-mails: marc.salle@univ-angers.fr; sebastien.goeb@univ-angers.fr
[b] Dr. S. Pascal, Dr. O. Siri
Aix Marseille Univ, CNRS UMR 7325, Centre Interdisciplinaire de Nanoscience de Marseille (CINaM), Campus de Luminy, 13288 Marseille cedex 09, France
E-mails: olivier.siri@univ-amu.fr; pascal@cinam.univ-mrs.fr
[c] Dr. M. Elhabiri, V. Mazan
Université de Strasbourg, Université de Haute-Alsace, CNRS, LIMA, UMR 7042, Equipe Chimie Bioorganique et Médicinale, ECPM, 25 Rue Becquerel, 67000 Strasbourg, France
[d] Dr. V. Carré, Prof. F. Aubriet,
LCP-A2MC, FR 3624, Université de Lorraine, ICPM
1 Bd Arago, 57078 Metz Cedex 03, France
[e] Prof. Z. Voitenko, M. Dekhtiarenko
Taras Shevchenko National University of Kyiv, 64/13 Volodymyrska st., Kyiv 01033, Ukraine

Supporting information : https://chemistry-europe.onlinelibrary.wiley.com/doi/10.1002/chem.202103039

Herein, we report the synthesis of two self-assembled metalla-rectangles **Oxa$_2$BBI$_2$** and **Naph$_2$BBI$_2$** featuring the pH sensitive benzobisimidazole (**BBI**) unit which also incorporate two pyridine fragments able to coordinate the metal centers. These structures differ essentially by the distances separating both **BBI** ligands, a parameter which depends on the size of the bis-ruthenium complex spacer (**RuOxa** or **RuNaphto**) (**Erreur ! Source du renvoi introuvable.**). On this basis, it is worth mentioning that whilst the smaller rectangle **Oxa$_2$BBI$_2$** exists only as a discrete monomer species, the larger **Naph$_2$BBI$_2$** can dimerize to form the catenated **(Naph$_2$BBI$_2$)$_2$** structure. Remarkably, this responsive interlocked species is able to dissociate in response to three different types of chemical or physical stimuli: i) dilution, ii) addition of pyrene and iii) protonation of the benzobisimidazole sidewalls (**Erreur ! Source du renvoi introuvable.**).

The synthesis of ligand **BBI** was achieved by the condensation of two equivalents of 4-pyridinecarboxaldehyde with tetraaminobenzene tetrahydrochloride in presence of piperidine and under aerobic conditions. After 16 h in refluxing acetonitrile, the ligand was isolated as a yellow-orange powder in a 80% yield. The reaction between the **RuOxa**[20] complex and the **BBI** ligand was carried out in MeOD at C = 10^{-3} M (T = 50 °C) and followed by ^{1}H NMR spectroscopy. After 2 h, the reaction converged to a single species that could be isolated upon precipitation with *tert*-butyl methyl ether (MeO*t*Bu). The resulting set of ^{1}H NMR signals illustrates the symmetry of the resulting self-assembled structure (**Erreur ! Source du renvoi introuvable.**b). A ^{1}H DOSY NMR experiment (Figure S3) revealed the presence of a single species in solution with a diffusion coefficient of D = 3.9 × 10^{-10} m^2 s^{-1} in MeOD-*d*$_4$ at C = 10^{-3} M. A hydrodynamic radius of *ca.* 10 Å was estimated from the Stokes-Einstein equation,[21] a value which is compatible with the formation of the expected Ru_4L_2 complex **Oxa$_2$BBI$_2$**. Similarly, the reaction carried out between the **RuNaphto**[22] complex and ligand **BBI** in MeOD afforded the metalla-rectangle **Naph$_2$BBI$_2$** characterized by a symmetric ^{1}H NMR spectrum (Figure 2c). As expected, a slightly larger Stokes radius of *ca.* 11 Å was extracted from the ^{1}H DOSY NMR experiment carried out in MeOD at C = 10^{-3} M (Figure S6).

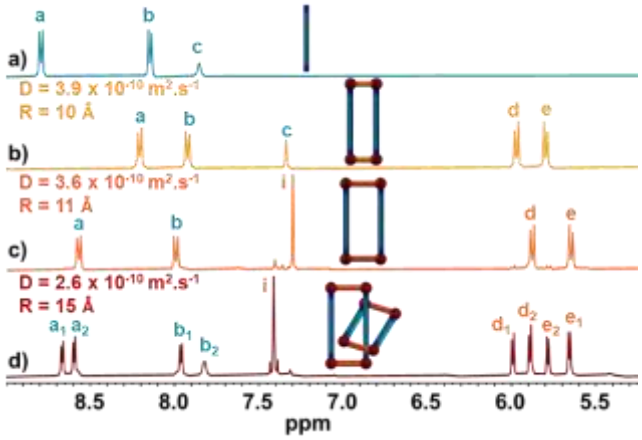

Figure 2. ^{1}H NMR (298 K, downfield region) of a) ligand **BBI** in DMSO-d$_6$, b) **Oxa$_2$BBI$_2$** in MeOD-*d*$_4$ (C = 10^{-3} M), c) **Naph$_2$BBI$_2$** in MeOD-*d*$_4$ (C = 10^{-3} M) and d) **(Naph$_2$BBI$_2$)$_2$** in MeOD-*d*$_4$ (C = 4 × 10^{-2} M). See **Erreur ! Source du renvoi introuvable.** for ^{1}H NMR assignments. D corresponds to the diffusion coefficient extracted from the ^{1}H DOSY NMR experiment and R to the corresponding hydrodynamic radius calculated from the Stokes-Einstein equation.

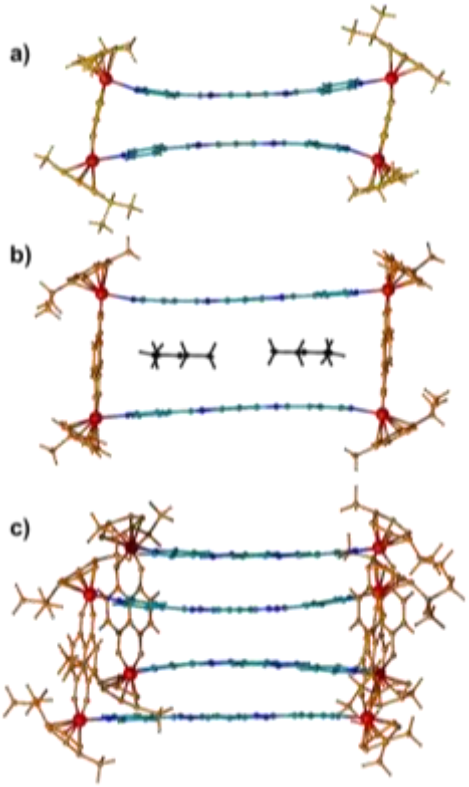

Figure 3. Single crystal X-ray diffraction structures of a) **Oxa$_2$BBI$_2$**, b) **Naph$_2$BBI$_2$** (including two solvent molecules, Et$_2$O) and c) MM+ simulation of **(Naph$_2$BBI$_2$)$_2$**. For a) and b) anions are omitted for clarity.

Single crystals of both metalla-rectangles were obtained by liquid diffusion of MeO*t*Bu or Et$_2$O into MeOH solutions (C = 10^{-3} M) containing **Oxa$_2$BBI$_2$** and **Naph$_2$BBI$_2$** respectively. X-ray crystallography confirmed unambiguously their Ru_4L_2 stoichiometry (**Erreur ! Source du renvoi introuvable.**a, **Erreur ! Source du renvoi introuvable.**b and S32). While both Ru atoms from a RuOxa complex are separated by 5.5 Å, π-π interactions occurring between face-to-face benzobisimidazole motifs lead to an interplanar distance of only 3.4 Å between the two central BBI units. Consequently, a significant bending occurs around the peripheral pyridine units, with a torsion of ca. 12° of the benzobisimidazole-pyridine junction. In contrast, **Naph$_2$BBI$_2$** shows a quasi-rectangular solid structure. Here, the larger distance which separates both **BBI** ligands (7.3 Å) does not allow π-π interactions between facing π-systems and is compensated by the accommodation of two Et$_2$O molecules in the central pocket.

High-resolution ESI-FTICR-HRMS spectrometry experiments were also carried out on **Oxa$_2$BBI$_2$** and **Naph$_2$BBI$_2$** in MeOH at C = 2 × 10^{-3} M (Figures S10-S12). While the reaction with **RuOxa** shows only signals corresponding to the monomer

system **Oxa$_2$BBI$_2$** at *m/z* = 630.7315 (3+) and 1020.5756 (2+) (main contributions, Figure S10), the species isolated from the reaction with the larger **RuNaphto** acceptor exhibits, under the same conditions, two sets of signals. They correspond to the monomeric metalla-rectangle **Naph$_2$BBI$_2$** with characteristic isotopic patterns at *m/z* = 697.4194 (3+) and 1120.6059 (2+) (main contributions), and to a dimeric **(Naph$_2$BBI$_2$)$_2$** structure with signals recorded at *m/z* = 1543.4649 (3+) and 1120.6059 (4+) (main contribution, Figures S11 and S12), respectively. In all cases, experimental isotopic distributions are in good agreement with theoretical ones.

On this basis, the ability of metalla-rectangle **Naph$_2$BBI$_2$** to dimerize was further investigated by concentration dependent ^{1}H NMR spectroscopy. Following Le Chatelier's principle, changing the concentration promotes the reversible conversion between the interlocked structure and the monomeric constitutive unit, thanks to the labile nature of the metal-ligand bonds and through-space interactions between the subunits.[11b] While only one set of ^{1}H NMR signals is observed at C = 10^{-3} M (**Erreur ! Source du renvoi introuvable.**c), the spectrum recorded at C = 4 × 10^{-2} M (**Erreur ! Source du renvoi introuvable.**d and S7) shows the splitting of the pyridine units (*a* and *b* protons), the *para*-cymene moieties (*d* and *e* protons) and the naphtoquinonato groups (*i* protons) signals, in accordance with the quantitative formation of the dimeric interlocked species **(Naph$_2$BBI$_2$)$_2$**.[11a] The corresponding ^{1}H DOSY NMR measurement confirmed the larger size of the resulting structure with a calculated hydrodynamic radius of *ca.* 15 Å (T = 298 K) (Figure S9). Formation of Borromean rings can be ruled out because of the non-symmetrical character of the ^{1}H NMR spectra,[11a] and the distances ratio between the long and the short sides of the metalla-rectangle, which do not match with the rules proposed by G.-X. Jin.[11b] The slow equilibrium between the monomer and the dimer species at the NMR timescale, allowed for a straightforward quantification of the dimerization constant K_{dim} (MeOD) = 4.4(± 0.2) × 10^2 (Figure S13 and S14).[16a, 23]

Despite numerous attempts, no crystal of **(Naph$_2$BBI$_2$)$_2$** of sufficient quality to be analyzed by X-ray diffraction has been obtained. Molecular force field (MM+) studies were therefore undertaken to determinate the structure of this interlocked species (Figure 3c). This modeling shows that the two metallacyles interlock without distortion with inter-ligand distances of about 3.4 Å as expected for such π–π stacking interactions.[11a, 16a]

The stability of the dimeric **(Naph$_2$BBI$_2$)$_2$** assembly was further investigated upon pyrene complexation. Such an electron rich planar species is expected to fill the cavity of the metalla-rectangle while interacting with both facing electron-deficient benzobisimidazole units, to afford a more thermodynamically stable host-guest complex. The progressive addition of pyrene to a solution of **(Naph$_2$BBI$_2$)$_2$** at 10^{-2} M in MeOD was followed by ^{1}H NMR (Figure S15). Remarkably, addition of one equivalent of pyrene per metalla-rectangle unit was sufficient to drastically simplify the NMR spectrum, as a consequence of the dissociation of the dimeric structure attributed to the intercalation of pyrene between both **BBI** panels of **Naph$_2$BBI$_2$** (Figure 4a). This hypothesis was confirmed by ^{1}H DOSY NMR measurement (Figure S16) which clearly demonstrates a higher diffusion value of the resulting species (3.55 × 10^{-10} m² s^{-1}) when compared with **(Naph$_2$BBI$_2$)$_2$**, a value which now corresponds to the one reported for isolated **Naph$_2$BBI$_2$** ring (Figures 2c and S6). The binding capability of **Naph$_2$BBI$_2$** for pyrene was evaluated by a ^{1}H NMR Job plot analysis (Figures S20 and S22a) and a titration experiment at C = 10^{-3} M in MeOD-*d$_4$* (Figures S21 and S22b).[24] These measurements revealed the complexation of one pyrene unit in the cavity of **Naph$_2$BBI$_2$** with an association constant K_a = 3.0(±0.2) × 10^3.

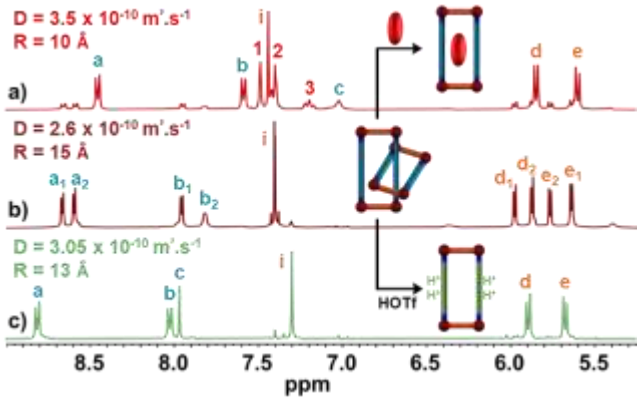

Figure 4. ^{1}H NMR spectra recorded in MeOD at C = 2 × 10^{-2} M of a) **(Naph$_2$BBI$_2$)$_2$** in presence of 1 equiv. of pyrene, b) **(Naph$_2$BBI$_2$)$_2$** and c) **(Naph$_2$BBI$_2$)$_2$** in presence of 6 equiv. of HOTf.

The optical properties of the ligand and both metalla-macrocycles were then investigated in methanol solutions. While **BBI** shows an absorption maximum at 358 nm (Figure 5a), the corresponding ligand-centered transitions are found at 393 and 386 nm for **Oxa$_2$BBI$_2$** and **Naph$_2$BBI$_2$**, respectively. These bands show more than doubled molar extinction coefficients (89 000 < ε < 101 000 M^{-1} cm^{-1}) compared to the free ligand (ε = 38 000 M^{-1} cm^{-1}). The red shift triggered by the coordination of the terminal pyridine units to ruthenium atoms is consistent with the one measured upon protonation of the **BBI** ligand in acidic medium (λ_{max} = 386 nm, Figure S33). To gain information into the stability of the complexes, their electronic absorption spectra were monitored over time at different concentrations (Figure S34). At C = 2 × 10^{-4} M, both **Oxa$_2$BBI$_2$** and **Naph$_2$BBI$_2$** complexes show unaltered absorptions after several days in solution. In contrast, for C ≤ 2 × 10^{-5} M, an hypsochromic shift is observed after 24 h, corresponding to the release of uncomplexed ligand in solution.

A strong emission of the **BBI** ligand was measured in the UV-blue region (Figure 5a), with a maximum centered at 430 nm and a fluorescence quantum yield of 40%. For both metalla-macrocycles recorded in fresh solutions at C = 2 × 10^{-5} M, weaker emissions are observed at around 460 nm, which is consistent with the fluorescence of recently reported tetranuclear Zn-benzobisimidazoles grid complexes.[25] However, when decreasing the concentration to C = 10^{-6} M, the emission is blue-shifted to 430 nm and most likely corresponds to the free ligand in solution (Figure S35) as already observed by absorption spectrophotometry.[26]

Complexation properties of **Naph$_2$BBI$_2$** were further investigated by UV-vis and fluorescence spectroscopy. The absorption and emission spectra of 1:1 mixture solutions of **BBI, Oxa$_2$BBI$_2$** or **Naph$_2$BBI$_2$** with pyrene were compared at C = 2 × 10^{-5} M (Figures

5b, S36 and S37). As expected, all absorption spectra show an additive effect between the two constituents. On the other hand, while the emission spectra corresponding to the mixture of **Naph$_2$BBI$_2$** and pyrene reveal a quasi-complete quenching of the pyrene emission (85 % decrease in the total fluorescence), a much weaker decrease of 21% and 33% is observed in the presence of **Oxa$_2$BBI$_2$** or **BBI** ligand respectively (Figures 5b and S37) illustrating the interaction of pyrene with the cavity of **Naph$_2$BBI$_2$**.[27]

The acid-base properties of the **BBI** ligand and the **Naph$_2$BBI$_2$** metalla-rectangle were then investigated using UV-visible absorption titrations as a function of pH (Figures S38-S44). The **BBI** ligand is characterized by 6 pH sensitive reactive sites, i.e. two on each imidazole units and one per pyridyl fragment (Figure S38). Figure S39 illustrates the spectral variations recorded during absorption spectrophotometric titration of **BBI** as a function of pH, which are in agreement with reported results on 4-pyridylbenzimidazole (4PBI).[28] Under neutral pH conditions (MeOH/H_2O 80/20 w/w, Figure S39), **BBI** is characterized by an intense absorption band in the UV region centered at 357 nm (ε^{357} = 3.50 × 10^4 M^{-1} cm^{-1}) in agreement with the data recorded in methanol. Increasing the pH from ~6.5 to ~11.9 induces a bathochromic shift of 23 nm of the π–π* transitions. The statistical processing of these data led to the determination of a pKa value of 11.2 ± 0.1 that is ascribed to the deprotonation of one of the two N1-imidazole sites (i.e., the pKa value for the deprotonation of the second N1-H function was estimated to be > 12 and could not be determined under our experimental conditions). On the other hand, the decrease in pH from ~ 6 to ~ 2.3 also leads to a bathochromic shift. Two pKa values of 3.7 ± 0.1 and 2.7 ± 0.1 were calculated (Figure S38). The two other pKa values were estimated to be < 2 in agreement with repulsive interactions between the various positively charged species. The neutral **BBI** ligand thus predominates over a broad range of pH (from ~4.5 to ~10.2) and can lead to **BBI^{4+}** and **BBI^{2-}** under strongly acidic and basic conditions, respectively.

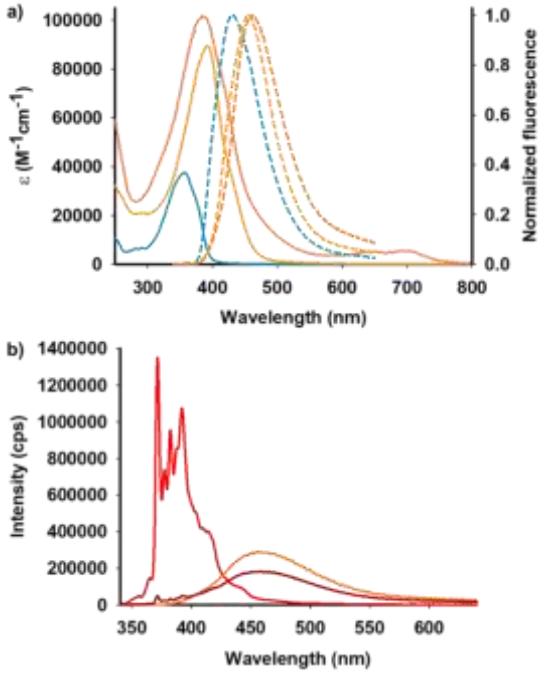

Figure 5. a) Electronic absorption (solid line) and emission (dashed line) spectra of **BBI** (C = 2 x 10^{-5} M), **Oxa$_2$BBI$_2$** and **Naph$_2$BBI$_2$** (C = 2 x 10^{-4} M for absorption and C = 2 x 10^{-5} M for emission) in methanol and b) fluorescence spectra recorded under the same experimental conditions of pyrene, **Naph$_2$BBI$_2$** and 1:1 mixture of both compounds in methanol (C = 2 x 10^{-5} M and λ_{ex} = 330 nm).

Since protons can compete for Lewis base pyridine sites in coordination self-assembled structures, acidic conditions often lead to a disassembly process.[17] We therefore investigated the pH-responsive behavior of the **Naph$_2$BBI$_2$** metalla-rectangle with the hypothesis that the presence of the imidazole moieties would allow for a selective protonation of the ligands without disassembly. Under neutral pH conditions (MeOH/H_2O 80/20 *w/w*), **Naph$_2$BBI$_2$** is characterized by an intense absorption in the UV region centered at 386 nm (ε^{386} = 8.88 x 10^4 M^{-1} cm^{-1}) assigned to π-π* ligand-localized transitions as well as a set of much weaker absorptions at 643 and 693 nm that correspond to LMCT transitions (i.e., signature of the metalla-rectangle).[22] Upon complexation to **RuNaphto**, the π–π* transitions of the two **BBI** ligands undergo significant bathochromic and hyperchromic shits ($\Delta\lambda$ ~29 nm; **BBI**: ε^{357} = 3.50 × 10^4 M^{-1} cm^{-1}; **Naph$_2$BBI$_2$**: ε^{386} = 8.88 × 10^4 M^{-1} cm^{-1}). Similarly to the observations in MeOH, the effect of complexation to the Ru centers by the terminal pyridines is comparable to that of their protonation (Figure S41, λ = 389 nm and ε^{389} = 2.68 × 10^4 M^{-1} cm^{-1}). The absorption *versus* pH titrations demonstrate that no decomposition of **Naph$_2$BBI$_2$** occurs over a large range of pH (2.20 – 12.05) as assessed by the ongoing presence of the LMCT signature. The statistical analysis of the data allowed evidencing two pH regions of interest (Figures S42-S44). Under strongly acidic conditions, the **Naph$_2$BBI$_2$** metalla-rectangle can undergo four protonation equilibria at its four equivalent N3-imidazole sites and three protonation constants could be accurately determined (pK_{a4} = 2.7 ± 0.2 and pK_{a3} + pK_{a2} = 4.5 ± 0.2). The protonation of these units results in only small

spectral variations both of the π–π* and LMCT transitions. In addition, the calculated pK_a values are lowered compared to those of the free **BBI** ligand (pK_{a3} = 2.7 ± 0.1 and pK_{a4} = 3.7 ± 0.1) due to the coordination of the pyridine units to the **RuNaphto** metal centers. These data therefore demonstrate that the **Naph$_2$BBI$_2$** meta-rectangle can undergo stepwise protonation on each of its N_3-imidazole units without any apparent signs of structural disassembly. Likewise, each of the N_1-imidazole units can undergo a deprotonation reaction without also affecting the architecture of the metallo-rectangle itself. Four deprotonation constants were determined under basic conditions (Figure S44). In contrast to acidic conditions, deprotonation of N_1-imidazole units is accompanied by strong spectral variations in both intra-ligand π–π* transitions (λ = 426 nm and $\varepsilon^{426} = 7.22 \times 10^4$ M^{-1} cm^{-1} for **Naph$_2$BBI$_2$**-4H) and LMCT transitions (hypsochromic shifts of ~60 nm; Figure S43).

On the basis of this in-depth investigation and considering the stability of cage **Naph$_2$BBI$_2$** in acidic media, we then studied by ^{1}H NMR and DOSY NMR the behavior of interlocked **(Naph$_2$BBI$_2$)$_2$** in presence of trifluoromethanesulfonic acid (HOTf). We hypothesized that protonation of the **BBI** moieties may lead to intermolecular electrostatic repulsions that could strongly affect the stability of the interlocked structure. Remarkably, addition of HOTf (6 equivalents per metallacycle) into a solution of **(Naph$_2$BBI$_2$)$_2$** in MeOD-*d$_4$* at C = 2×10^{-2} M produces quantitatively a new species (Figures 4c and S23). It shows a higher D value and non-splitted NMR signals that are downfield shifted in comparison to those of the dimeric structure (Figure 4b). These NMR characteristics support the dissociation of the protonated **(Naph$_2$BBI$_2$)$_2$** interlocked dimer and formation of the **Naph$_2$BBI$_2$H$_4$** monomer. This was unambiguously demonstrated through a comparative NMR study with **Naph$_2$BBI$_2$** recorded in a 0.12 M solution of HOTf in MeOD at C = 10^{-3} M (Figures S24 and S25) and ESI-FTICR HRMS measurements (Figure S26). Finally, it is worth noting that this original dissociation phenomenon is reversible, since addition of 6 equivalents of *N*,*N*-diisopropylethylamine (DIPEA) reforms quantitatively the starting interlocked species (Figure S23).
Finally, we investigated the complexation ability of **Naph$_2$BBI$_2$H$_4$** toward the electron rich pyrene unit. Since protonation of the **BBI** units increases their electron deficient character, we expected **Naph$_2$BBI$_2$H$_4$** to be a better host for pyrene than **Naph$_2$BBI$_2$**. This was confirmed by a ^{1}H NMR titration recorded at C = 10^{-3} M in a solution of HOTf (C = 6×10^{-3} M) in MeOD-*d$_4$* (Figures S22 and S27). An association constant K_a = 1.32 (± 0.09) × 10^4 was measured, a value four times higher than the one calculated with the non-protonated **Naph$_2$BBI$_2$** host analog. Interestingly, this tunable binding affinity can be followed by ^{1}H NMR and DOSY NMR upon successive addition of HOTf and DIPEA (Figures S28-S31).

In summary, two novel self-assembled metalla-rectangles incorporating a pH sensitive benzobis(imidazole)-based ligand were designed. Thanks to the reversible nature of the coordination bonds and favorable electronic interactions, the larger **Naph$_2$BBI$_2$** which shows an interplanar distance of 7.3 Å between both ligand units can be quantitatively transformed to the interlocked molecular structure **(Naph$_2$BBI$_2$)$_2$** in MeOH at C = 2×10^{-2} M. Remarkably, this stimuli responsive interpenetrated catenane can be dissociated in three different ways: i) upon dilution to a concentration of C = 1 mM, ii) in the presence of pyrene, leading the 1:1 host-guest complex pyrene⊂**Naph$_2$BBI$_2$** and iii) by selectively protonating the N_3-imidazole basic sites with HOTf to form the charged **Naph$_2$BBI$_2$H$_4$** metalla-rectangle. Importantly this can be accomplished without any trace of disassembled species as usually observed under acidic conditions and reversibly through addition of DIPEA.

Deposition numbers 2096156 (**Oxa$_2$BBI$_2$**), and 2096158 (for **Naph$_2$BBI$_2$**) contain the supplementary crystallographic data for this paper. These data are provided free of charge by the joint Cambridge Crystallographic Data Centre and Fachinformationszentrum Karlsruhe Access Structures service www.ccdc.cam.ac.uk/structures.

Acknowledgements

The authors gratefully acknowledge the French Embassy in Kiev (Ukr) for PhD grant (MD). They also acknowledge the ASTRAL platform (SFR MATRIX, Univ. Angers) for their assistance in spectroscopic analyses and the French national FT-ICR network for its financial support (FR 3624 CNRS).

Keywords: Benzobis(imidazole) • Host–guest systems • Metalla-cycles • Self-assembly • pH • Catenation

[1] Y. Sun, C. Chen, J. Liu, P. J. Stang, *Chem. Soc. Rev.* **2020**, *49*, 3889–3919.

[2] a) F. J. Rizzuto, L. K. S. von Krbek, J. R. Nitschke, *Nat. Rev. Chem.* **2019**, *3*, 204–222; b) Y. Han, Y. Tian, Z. Li, F. Wang, *Chem. Soc. Rev.* **2018**, *47*, 5165–5176; c) V. A. Azov, *Tetrahedron Lett.* **2016**, *57*, 5416–5425; d) S. Zarra, D. M. Wood, D. A. Roberts, J. R. Nitschke, *Chem. Soc. Rev.* **2015**, *44*, 419–432.

[3] a) A. B. Grommet, M. Feller, R. Klajn, *Nat. Nanotechnol.* **2020**, *15*, 256–271; b) Y. Fang, J. A. Powell, E. Li, Q. Wang, Z. Perry, A. Kirchon, X. Yang, Z. Xiao, C. Zhu, L. Zhang, F. Huang, H.-C. Zhou, *Chem. Soc. Rev.* **2019**, *48*, 4707–4730; c) M. D. Pluth, R. G. Bergman, K. N. Raymond, *Acc. Chem. Res.* **2009**, *42*, 1650–1659; d) H. Amouri, C. Desmarets, J. Moussa, *Chem. Rev.* **2012**, *112*, 2015–2041; e) M. Yoshizawa, J. K. Klosterman, M. Fujita, *Angew. Chem. Int. Ed.* **2009**, *48*, 3418–3438.

[4] a) M. L. Saha, X. Yan, P. J. Stang, *Acc. Chem. Res.* **2016**, *49*, 2527–2539; b) L. Xu, Y.-X. Wang, H.-B. Yang, *Dalton Trans.* **2015**, *44*, 867–890.

[5] A. Casini, B. Woods, M. Wenzel, *Inorg. Chem.* **2017**, *56*, 14715–14729.

[6] a) W. X. Gao, H. J. Feng, B. B. Guo, Y. Lu, G. X. Jin, *Chem. Rev.* **2020**, *120*, 6288–6325; b) Y. Lu, D. Liu, Y.-J. Lin, Z.-H. Li, G.-X. Jin, *Natl. Sci. Rev.* **2020**, *7*, 1548–1556; c) G. Gil-Ramírez, D. A. Leigh, A. J. Stephens, *Angew. Chem. Int. Ed.* **2015**, *54*, 6110–6150.

[7] a) M. Siddiqui, R. Saha, P. S. Mukherjee, *Inorg. Chem.* **2019**, *58*, 4491–4499; b) J. Singh, D. H. Kim, E.-H. Kim, N. Singh, H. Kim, R. Hadiputra, J. Jung, K.-W. Chi, *Chem. Commun.* **2019**, *55*, 6866–6869; c) J.-H. Jo, N. Singh, D. Kim, S. M. Cho, A. Mishra, H. Kim, S. C. Kang, K.-W. Chi, *Inorg. Chem.* **2017**, *56*, 8430–8438; d) H. Lee, P. Elumalai, N. Singh, H. Kim, S. U. Lee, K. W. Chi, *J. Am. Chem. Soc.* **2015**, *137*, 4674–4677; e) A. Mishra, A. Dubey, J. W. Min, H. Kim, P. J. Stang, K.-W. Chi, *Chem. Commun.* **2014**, *50*, 7542–7544.

[8] a) N. Singh, D. Kim, D. H. Kim, E.-H. Kim, H. Kim, M. S. Lah, K.-W. Chi, *Dalton Trans.* **2017**, *46*, 571–577; b) V. Vajpayee, Y. H. Song, T. R. Cook, H. Kim, Y. Lee, P. J. Stang, K.-W. Chi, *J. Am. Chem. Soc.* **2011**, *133*, 19646–19649.

[9] a) Z. Cui, Y. Lu, X. Gao, H.-J. Feng, G.-X. Jin, *J. Am. Chem. Soc.* **2020**, *142*, 13667–13671; b) H.-N. Zhang, W.-X. Gao, Y.-J. Lin,

G.-X. Jin, *J. Am. Chem. Soc.* **2019**, *141*, 16057–16063; c) Y. H. Song, N. Singh, J. Jung, H. Kim, E.-H. Kim, H.-K. Cheong, Y. Kim, K.-W. Chi, *Angew. Chem. Int. Ed.* **2016**, *55*, 2007–2011; d) J. E. Beves, J. J. Danon, D. A. Leigh, J.-F. Lemonnier, I. J. Vitorica-Yrezabal, *Angew. Chem. Int. Ed.* **2015**, *54*, 7555–7559; e) C. Schouwey, J. J. Holstein, R. Scopelliti, K. O. Zhurov, K. O. Nagornov, Y. O. Tsybin, O. S. Smart, G. Bricogne, K. Severin, *Angew. Chem. Int. Ed.* **2014**, *53*, 11261–11265; f) C. D. Pentecost, K. S. Chichak, A. J. Peters, G. W. V. Cave, S. J. Cantrill, J. F. Stoddart, *Angew. Chem. Int. Ed.* **2007**, *46*, 218–222.

[10] a) L.-L. Dang, X. Gao, Y.-J. Lin, G.-X. Jin, *Chem. Sci.* **2020**, *11*, 1226–1232; b) S. D. P. Fielden, D. A. Leigh, S. L. Woltering, *Angew. Chem. Int. Ed.* **2017**, *56*, 11166–11194; c) L.-L. Dang, Z.-B. Sun, W.-L. Shan, Y.-J. Lin, Z.-H. Li, G.-X. Jin, *Nat. Commun.* **2019**, *10*, 1–9; d) B.-B. Guo, Y.-J. Lin, G.-X. Jin, *Chem. Eur. J.* **2019**, *25*, 9721–9727.

[11] a) H.-J. Feng, W.-X. Gao, Y.-J. Lin, G.-X. Jin, *Chem. Asian J.* **2019**, *14*, 2712–2718; b) Y. Lu, H.-N. Zhang, G.-X. Jin, *Acc. Chem. Res.* **2018**, *51*, 2148–2158; c) Y. Lu, Y. Lin, Z. Li, G. Jin, *Chin. J. Chem* . **2018**, *36*, 106–111; d) H.-N. Zhang, W.-X. Gao, Y.-X. Deng, Y.-J. Lin, G.-X. Jin, *Chem. Commun.* **2018**, *54*, 1559–1562; e) Y. Lu, Y.-X. Deng, Y.-J. Lin, Y.-F. Han, L.-H. Weng, Z.-H. Li, G.-X. Jin, *Chem* **2017**, *3*, 110–121; f) T. Kim, N. Singh, J. Oh, E.-H. Kim, J. Jung, H. Kim, K.-W. Chi, *J. Am. Chem. Soc.* **2016**, *138*, 8368–8371; g) S.-L. Huang, Y.-J. Lin, T. S. A. Hor, G.-X. Jin, *J. Am. Chem. Soc.* **2013**, *135*, 8125–8128.

[12] a) S.-L. Huang, T. S. A. Hor, G.-X. Jin, *Coord. Chem. Rev.* **2017**, *333*, 1–26; b) M. Frank, M. D. Johnstone, G. H. Clever, *Chem. Eur. J.* **2016**, *22*, 14104-14125.

[13] C. J. Bruns, J. F. Stoddart, *The Nature of the Mechanical Bond: From Molecules to Machines*, Wiley, Hoboken, NJ, USA, **2016**.

[14] W. Wang, Y.-X. Wang, H.-B. Yang, *Chem. Soc. Rev.* **2016**, *45*, 2656–2693.

[15] S. J. Wezenberg, *Chem. Lett.* **2020**, *49*, 609–615.

[16] a) S. Krykun, M. Dekhtiarenko, D. Canevet, V. Carré, F. Aubriet, E. Levillain, M. Allain, Z. Voitenko, M. Sallé, S. Goeb, *Angew. Chem. Int. Ed.* **2020**, *59*, 716–720; b) G. Szalóki, S. Krykun, V. Croué, M. Allain, Y. Morille, F. Aubriet, V. Carré, Z. Voitenko, S. Goeb, M. Sallé, *Chem. Eur. J.* **2018**, *24*, 11273–11277.

[17] a) L. S. Lisboa, J. A. Findlay, L. J. Wright, C. G. Hartinger, J. D. Crowley, *Angew. Chem. Int. Ed.* **2020**, *59*, 11101–11107; b) I. A. Riddell, M. M. J. Smulders, J. K. Clegg, J. R. Nitschke, *Chem. Commun.* **2010**, *47*, 457–459; c) L. Xu, D. Zhang, T. K. Ronson, J. R. Nitschke, *Angew. Chem. Int. Ed.* **2020**, *59*, 7435–7438; d) S. Ganta, D. K. Chand, *Inorg. Chem.* **2018**, *57*, 3634–3645; e) J. J. Henkelis, J. Fisher, S. L. Warriner, M. J. Hardie, *Chem. Eur. J.* **2014**, *20*, 4117–4125; f) J. E. M. Lewis, E. L. Gavey, S. A. Cameron, J. D. Crowley, *Chem. Sci.* **2012**, *3*, 778–784; g) P. Mal, D. Schultz, K. Beyeh, K. Rissanen, J. R. Nitschke, *Angew. Chem. Int. Ed.* **2008**, *47*, 8297–8301.

[18] a) S. Goeb, M. Sallé, *Acc. Chem. Res.* **2021**, *54*, 1043–1055; b) T. Y. Kim, R. A. S. Vasdev, D. Preston, J. D. Crowley, *Chem. Eur. J.* **2018**, *24*, 14878–14890; c) G. Szalóki, V. Croué, V. Carré, F. Aubriet, O. Alévêque, E. Levillain, M. Allain, J. Arago, E. Orti, S. Goeb, M. Sallé, *Angew. Chem. Int. Ed.* **2017**, *56*, 16272–16276; d) V. Croué, S. Goeb, G. Szalóki, M. Allain, M. Sallé, *Angew. Chem. Int. Ed.* **2016**, *55*, 1746–1750; e) A. K.-W. Chan, W. H. Lam, Y. Tanaka, K. M.-C. Wong, V. W.-W. Yam, *Proc. Natl. Acad. Sci.* **2015**, *112*, 690–695.

[19] S. Jansze, K. Severin, *J. Am. Chem. Soc.* **2019**, *141*, 815–819.

[20] H. Yan, G. Süss-Fink, A. Neels, H. Stoeckli-Evans, *J. Chem. Soc., Dalton Trans.* **1997**, 4345–4350.

[21] a) L. Avram, Y. Cohen, *Chem. Soc. Rev.* **2015**, *44*, 586–602; b) A. Macchioni, G. Ciancaleoni, C. Zuccaccia, D. Zuccaccia, *Chem. Soc. Rev.* **2008**, *37*, 479–489.

[22] N. P. E. Barry, J. Furrer, B. Therrien, *Helv. Chim. Acta* **2010**, *93*, 1313–1328.

[23] L. Faour, C. Adam, C. Gautier, S. Goeb, M. Allain, E. Levillain, D. Canevet, M. Sallé, *Chem. Commun.* **2019**, *55*, 5743–5746.

[24] a) G. Bastien, P. I. Dron, M. Vincent, D. Canevet, M. Allain, S. Goeb, M. Sallé, *Org. Lett.* **2016**, *18*, 5856–5859; b) D. Canevet, M. Gallego, H. Isla, A. de Juan, E. M. Perez, N. Martin, *J. Am. Chem. Soc.* **2011**, *133*, 3184–3190.

[25] B. Schäfer, N. Suryadevara, J.-F. Greisch, O. Fuhr, M. M. Kappes, M. Ruben, *Eur. J. Org. Chem.* **2021**, *2021*, 2301–2310.

[26] No quantum yield could be accurately determined due to the poor stability of the complexes at the concentration requested for the measurements.

[27] Decrease in emission was evaluated by comparing the emission aera of a 1:1 mixture of pyrene and **BBI**, **Oxa$_2$BBI** or **Naph$_2$BBI**, with the additiion of emission aeras of pyrene and **BBI**, **oxa$_2$BBI** and **Naph$_2$BBI** respectively, recorded in the same conditions.

[28] a) N. Singhal, A. Mishra, A. Datta, *ChemPhysChem* **2016**, *17*, 3004–3009; b) V. Khorwal, A. Datta, *J. Photochem. Photobiol., A* **2012**, *250*, 99–102; c) M. Novo, M. Mosquera, F. Rodriguez Prieto, *J. Phys. Chem.* **1995**, *99*, 14726–14732; d) M. Novo, M. Mosquera, F. R. Prieto, *Can. J. Chem.* **1992**, *70*, 823–827.